Astrochemistry VII – Through the Cosmos
from Galaxies to Planets
Proceedings IAU Symposium No. 332, 2017
M. Cunningham, T. Millar & Y. Aikawa, eds.

doi:10.1017/S1743921317007864

Photodissociation processes of Bisanthenquinone cation

Tao Chen[1,2], Junfeng Zhen[2,3], Ying Wang[1], Harold Linnartz[3] and Alexander G. G. M. Tielens[2]

[1]Department of Theoretical Chemistry and Biology, School of Biotechnology, Royal Institute of Technology, 10691, Stockholm, Sweden
[2]Leiden University, Leiden Observatory, Niels Bohrweg 2, NL-2333 CA Leiden, Netherlands
[3]Sackler Laboratory for Astrophysics, Leiden Observatory, University of Leiden, P.O. Box 9513, 2300 RA Leiden, The Netherlands
email: chen@strw.leidenuniv.nl

Abstract. A systematic study, using ion trap time-of-flight mass spectrometry, is presented for the photo-dissociation processes of Bisanthenquinone (Bq) cations, $C_{28}H_{12}O_2{}^+$, a ketone substituted Polycyclic Aromatic Hydrocarbon (PAH). The Bq cation fragments through sequential loss of the two neutral carbonyl (CO) units upon laser (626nm) irradiation, resulting in a PAH-like derivative $C_{26}H_{12}{}^+$. Upon further irradiation, $C_{26}H_{12}{}^+$ exhibits both stepwise dehydrogenation and C_2/C_2H_2 loss fragmentation channels. Quantum chemistry calculations reveal a detailed picture for the first CO-loss, which involves a transition state with a barrier of $\sim$ 3.4 eV, which is lower than the energy required for the lowest H-loss pathway ($\sim$ 5.0 eV). The barrier for the second CO-loss is higher ($\sim$ 4.9 eV). The subsequent loss of this unit changes the Bq geometry from a planar to a bent one. It is concluded that the photodissociation mechanism of the substituted PAH cations studied here is site selective in the substituted subunit. This work also shows that an acetone substituted PAH cation is not photo-stable upon irradiation.

Keywords. PAH, molecule, photodissociation, quinone, carbonyl, TOF

1. Introduction

Bisanthenquinone (Bq) molecules are commonly referred to as Polycyclic Aromatic Hydrocarbon (PAH) quinones. They form a subclass within the PAH family, molecules that are important from a physical chemical point of view and that also act as an important component of the interstellar medium (ISM) (Tielens (2008)). The vibrational signatures of PAHs dominate the mid-infrared spectra of most objects in space and they are key contributors to the energy and ionization balance of the gas. These PAHs are thought to form in stellar ejecta. Subsequently they are further processed for some hundred million years in the harsh environment of the ISM (Tielens (2005)). As part of this evolution, PAHs may acquire functional groups such as methyl, methoxy, and hydroxyl groups (Bernstein *et al.* (2002)). Little information is available on how photolysis affects substituted derivatives of PAH cations (Jochims *et al.* (1999), Rapacioli *et al.* (2015)). Such species contain highly active reaction centers that will affect the photodissociation efficiency and photoisomerization process (Lifshitz (1997), Bernstein *et al.* (2002), Walsh (2008)). This has been studied for methyl- and methoxy-substituted derivatives of hexaperi-hexabenzocoronene (HBC) cations, i.e., $(OCH_3)_6HBC^+$ and $(CH_3)_4(OCH_3)_2HBC^+$ that dissociate through the loss of CH_3CO units upon laser (595 nm) irradiation, resulting in a PAH-like derivative $C_{36}H_{12}^+$ and a methyl-substituted PAH derivative $C_{44}H_{24}^+$,

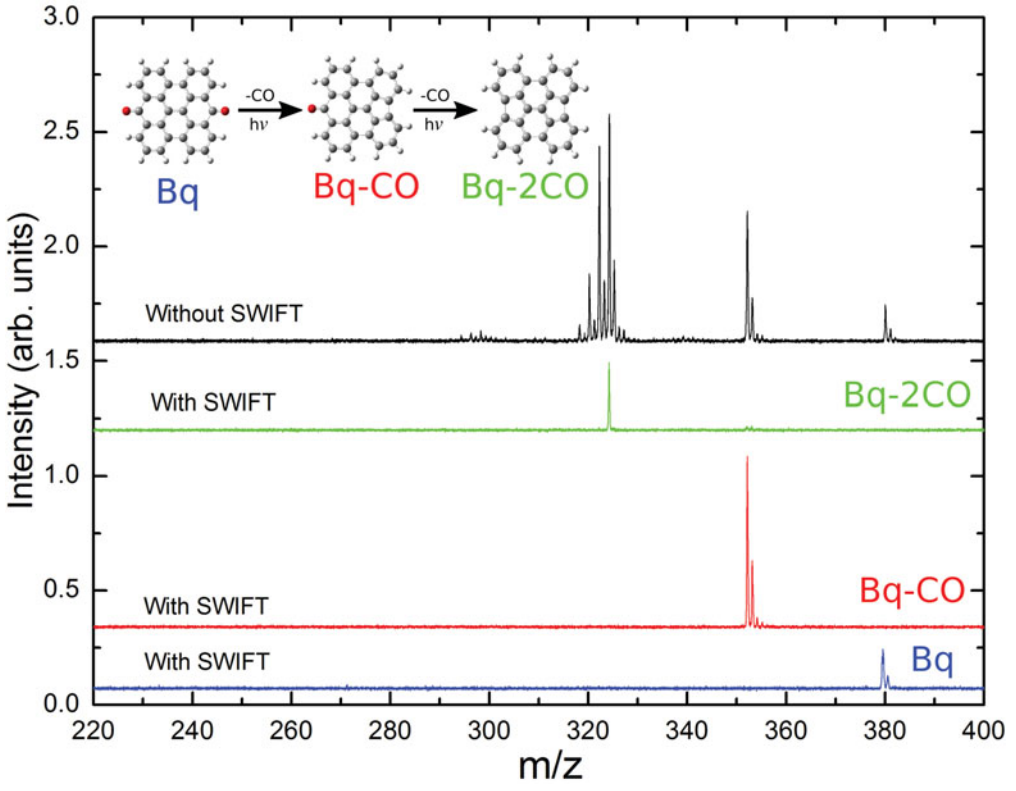

Figure 1. The mass spectrum of Bq cation, before (black curve) and after (green, red and blue curves) SWIFT signal isolation. The blue curve at mass 380.1 amu corresponds to the molecule as shown in the upper-left inset (Bq). The red curve at mass 352.1 amu corresponds to the molecule as shown in the upper-left inset (Bq-CO). The green curve at mass 324.1 amu corresponds to the molecule as shown in the upper-left inset (Bq-2CO). The small peaks on the right side of the main peak in graphs A and B are isotopic contributions from ^{13}C or ^{18}O. SWIFT isolation effectively excludes isotopes in the mass spectrum of Bq-2CO cation.

respectively (Zhen *et al.* (2016)). In this work, we present a study of Bq cations for understanding the effect of acetone site-substitution on photostability and reactivity behavior of PAHs and to elucidate the possible two step mechanism in the photolysis of methoxylated PAHs (e.g., loss of a CH_3 unit followed by CO elimination). The experiments are conducted by using quadrupole ion trap time-of-flight (QIT-TOF) mass spectrometry. Density functional theory (DFT) calculations are performed to explore the dissociation process of Bq cation.

2. Experimental setup

The experiments on photo-fragmentation processes of Bq cations are conducted with a quadrupole ion trap (QIT) time-of-flight (TOF) system: i-PoP (instrument for Photodissociation of PAHs) developed by Zhen *et al.* (2014). In general, it works in the following way: commercially available Bq powder (purity higher than 99.0 % from Kentax) is heated to $\sim$ 500 K in an oven. Subsequently, the evaporated molecules are ionized by an electron gun and guided into the ion trap. Once the ions are trapped, a Stored Waveform Inverse Fourier Transform (SWIFT) excitation technique developed by Doroshenko & Cotter (1996) is applied to isolate a specific range of mass/charge (m/z) species or a

https://doi.org/10.1017/S1743921317007864 Published online by Cambridge University Press

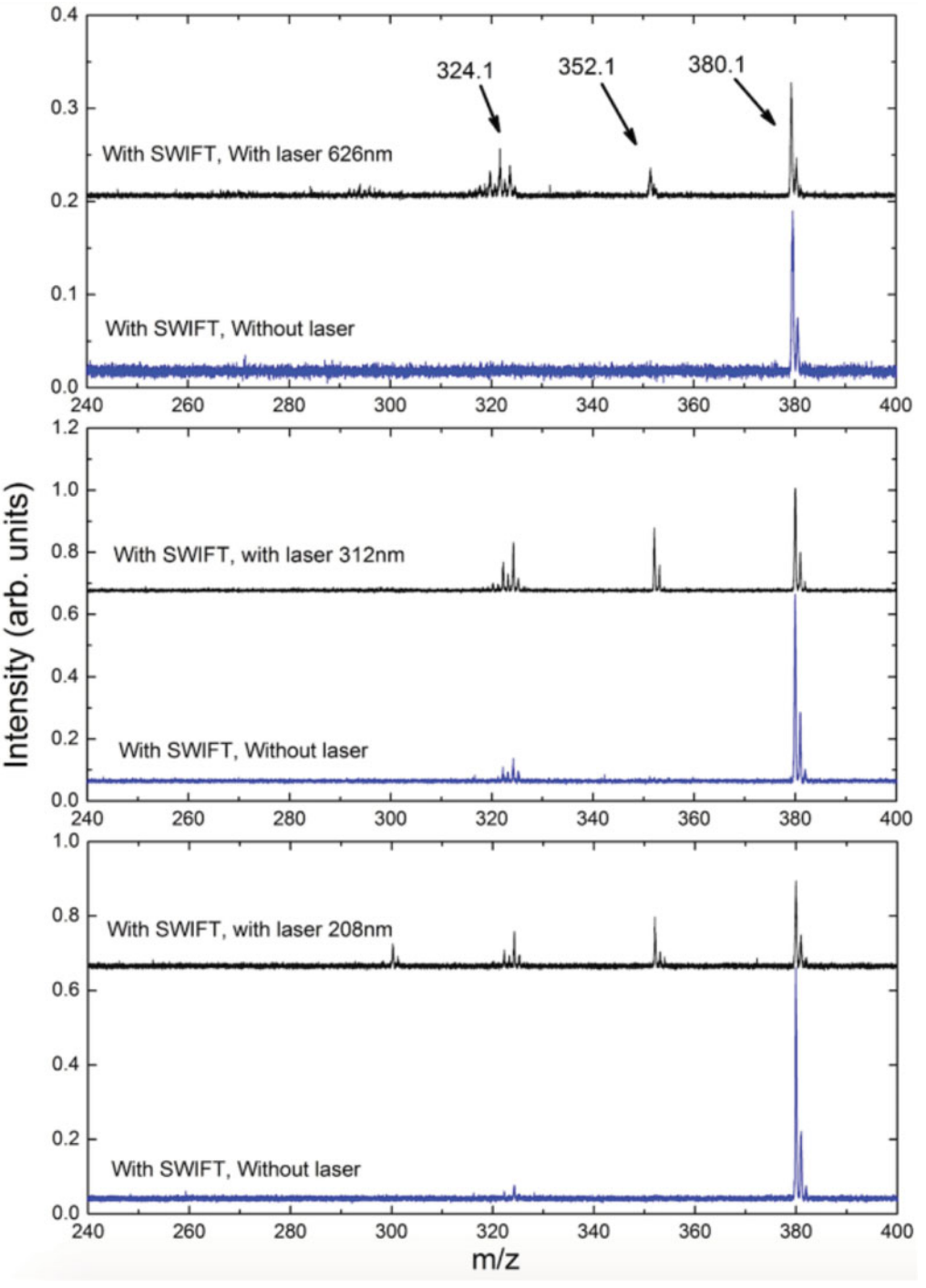

Figure 2. Mass-spectrum of Bq cation, before and after irradiation by 626 nm, 312 nm, and 208 nm laser light. Bq (380.1 amu) is dissociated to Bq-CO (352.1 amu) and Bq-2CO (324.1 amu) at all given wavelength. The black curves represent the selected molecules with SWIFT and with irradiation of laser. The blue curves are SWIFT selected Bq without laser irradiation. No other peaks are observed at Bq and Bq-CO except isotopes, meaning that CO is the dominant dissociation channel for Bq and Bq-CO.

https://doi.org/10.1017/S1743921317007864 Published online by Cambridge University Press

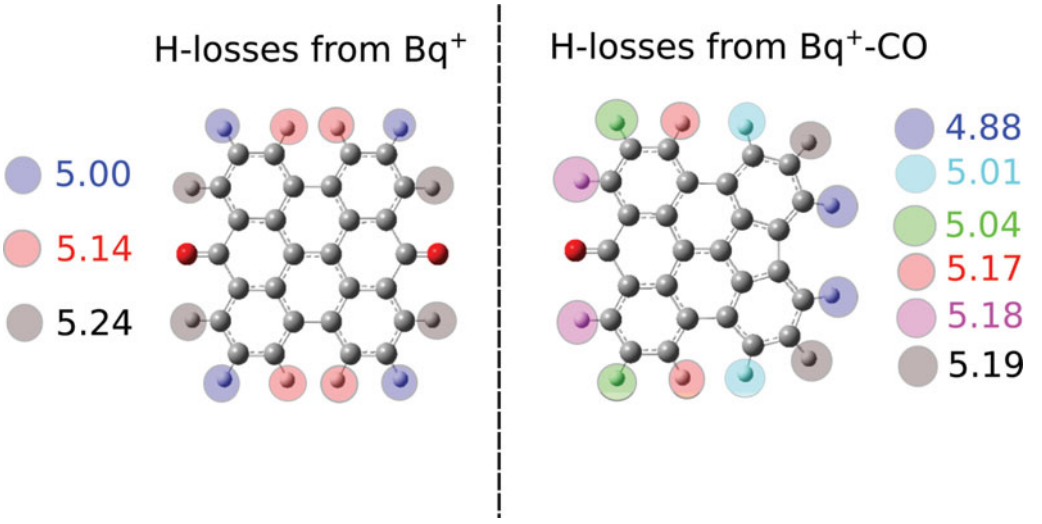

Figure 3. The dissociation energies for H-losses from Bq and Bq-CO cation. All values are given in eV.

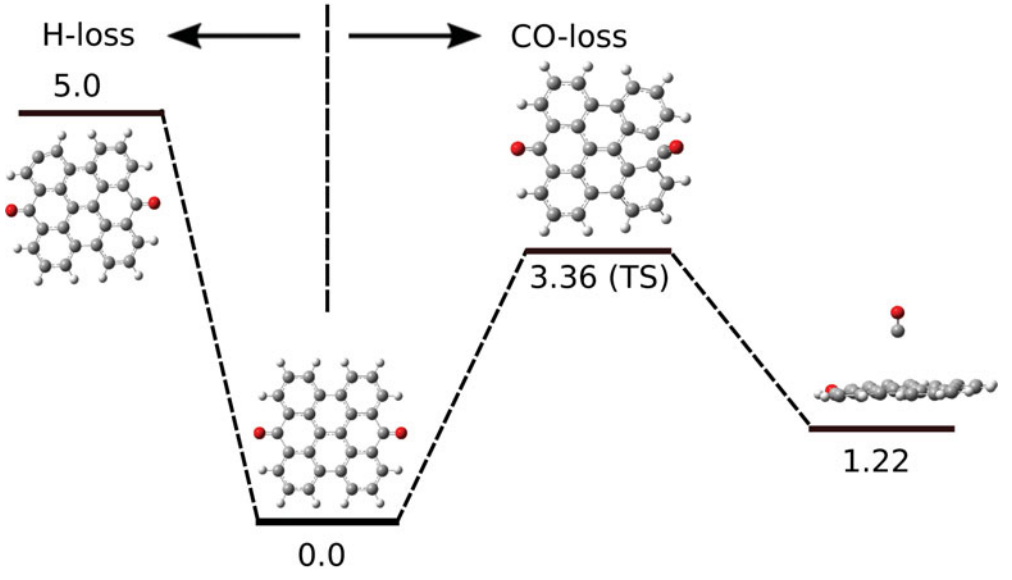

Figure 4. Calculated dissociation energies and reaction barriers for H-loss and first CO-loss from Bq cation. All values are given in eV.

single peak species (i.e. $^{12}C_{26}H_{12}{}^{+}$). After a short time delay (typically $\sim$ 0.2s), the ion cloud is cooled down to room temperature ($\sim$ 298K) due to collisions with He buffer gas that is continuously added to the trap. Subsequently, the ion cloud is irradiated by the light pulses generated by a tunable dye laser (LIOP-TEC, Quasar2-VN) pumped by a Nd:YAG laser (DCR-3, Spectra-Physics), operated at 10Hz. DCM is used to produce 626 nm light as well as 312 and 208 nm radiation through doubling and tripling. As no clear wavelenghth dependency is found, we only present the results obtained upon 626 nm irradiation. The fragments or intact molecules after irradiation are accelerated by a

https://doi.org/10.1017/S1743921317007864 Published online by Cambridge University Press

negative square pulse to transport them from the trap to the field-free TOF region. The signals are finally detected by a MicroChanel Plates (MCP) detector.

3. Computational methods

Our theoretical calculations are carried out using DFT. The dissociation energies, transition state energies and charge distributions presented in this work are calculated using the hybrid density functional B3LYP method as implemented in the Gaussian 09 program. All structures are optimized using the 6-31G(d) basis set. The vibrational frequencies are calculated to confirm that the structures correspond to minima (no imaginary frequencies) or transition states (one imaginary frequency). We have taken the Zero Point Vibrational Energy (ZPVE) into account. The ZPVE values are scaled by the empirical factor 0.9806 from Scott & Radom (1996) to correct for anharmonic effects. The Potential Energy Surface (PES) of all possible dissociation pathways is scanned for transition state calculations. Intrinsic reaction coordinate calculations are performed to confirm that the transition state structures are connected to their corresponding local minima.

4. Results and Discussion

Figure 1 shows the mass spectrum of the trapped Bq cations. The top mass spectrum is obtained without laser irradiation and without SWIFT signal isolation. It illustrates by Beynon *et al.* (1959) that the parent cations experience substantial fragmentation due to the electron impact ionization. The improvement in mass purity becomes clear from the lower three curves, where mass peaks at m/z=380.1 for the precursor species (Bq cation), at 352.1 for the first photofragment (Bq-CO cation) and at 324.1 for the second photofragment (Bq-2CO cation) are shown using the SWIFT pulse isolation. The mass spectra of Bq and Bq-CO cation show that the relatively small isotopic contributions from ^{13}C or ^{18}O, at m/z = 381.1 & 382.1 and 353.1 & 354.1 are suppressed effectively by the SWIFT pulse. Isolation of the parent mass peak, excludes ^{13}C contributions in the mass spectrum of Bq-2CO cation.

Figure 2 shows the mass-spectrum of Bq cation, before and after irradiation by 626 nm, 312 nm, and 208 nm laser light. There exist no clear wavelength dependency and therefore below only the 626 nm data are presented. As shown in Figure 1, the precursor molecule is located at m/z=380.1. Two main fragments are found with peaks at m/z = 352.1 and 324.1. The separation between precursor and first fragment peak as well as between first and second fragment peak amounts to 28 Da mass differences. This corresponds to one oxygen plus one carbon, suggesting an effective CO unit (m/z = 28) fragmentation channel. Also these two peaks are separated by a 28 Da mass difference. Moreover, no other peaks are observed at Bq and Bq-CO except isotopes, the loss of hydrogens cannot be detected in the experiments. The interpretation of these observations is that Bq photofragmentation is governed by the sequential loss of the two CO units, transfering Bq into Bq-CO and Bq-2CO. It is interesting to note that this CO-loss channel is clearly preferred above dehydrogenation, i.e., fragmentation through H-atom loss. For many regular PAHs, i.e., PAHs without side group additions, H-loss and 2H/H_2-loss are dominant dissociation channels (Chen *et al.* (2015)). As reported by Zhen *et al.* (2016) PAHs with side group additions, other dissociation pathways have been found, e.g. methoxy groups.

Figure 3 shows calculated dissociation energies for all possible H-loss pathways from Bq and Bq-CO cation. In the Bq case, with its high level of symmetry, only three different

https://doi.org/10.1017/S1743921317007864 Published online by Cambridge University Press

types of H-atoms can be distinguished. The lowest dissociation energy for H-loss is found for H-atoms dissociating from the corner locations and amounts to 5.0 eV. For the Bq-CO cation the PAH geometry looses its symmetry and the lowest dissociation energy (4.88 eV) is now found for the two H-atoms that were closest to the lost CO-unit.

Figure 4 describes the CO and H dissociation pathways from Bq. The lowest dissociation pathway for H-loss is a one-step process without any transition state involved, and the calculated barrier is 5 eV. The CO-loss starts with the dissociation of one of the two C-C bonds (between Bq carbon and carbonyl). A transition state, in which the CO is connected with only one carbon atom of Bq, is formed by overcoming a barrier of 3.36 eV. The partially free CO in this intermediate can rotate along the binding carbon and upon breaking the bond, move out from the Bq-plane, resulting in the formation of a pentagon. Such process is similar to the photo-dissociation of methoxy-substituted derivatives of HBC cations Zhen *et al.* (2016), in which pentagons are formed after loss of a CH_3CO unit. The carbonyl keeps moving towards the center of the Bq-plane and it finally leaves vertically from the middle of the Bq-plane. Although the CO-loss pathway contains a transition state, the barrier is only 3.36 eV, which is much lower than the barrier of the H-loss (5 eV) from Bq. The loss of one CO-unit, therefore, is favoured above that of an H-atom, fully consistent with the experimental findings.

5. Conclusion

Experiments and quantum chemistry calculations are performed for understanding the photo-dissociation processes of Bq cations. The mass spectrum of Bq cation upon laser (626nm) irradiation presents clear evidence for pure neutral CO-losses, i.e., no other fragments are detected as a first or second dissociation product. Our quantum chemistry calculation reveals that for Bq the transition barrier for CO-loss is only ~ 3.4 eV, which is much lower than alternative routes. We expect that CO loss from larger PAH quinones will also lead to pentagon formation and we speculate that this will facilitate the isomerization of large PAHs to cages and fullerenes in the interstellar medium (Berné & Tielens(2012)).

The results reported here are interesting also from a different point of view. Pentagon formation is important to understand how PAHs can transfer into carbon cages and fullerenes, as proposed by Berné & Tielens(2012) and experimentally investigated by Zhen *et al.* (2014). Several pathways have been discussed, and a recent study by de Haas *et al.* (2017) show the facile pentagon formation upon irradiation of PAHs. Here it is shown that pentagon formation can also be initialized through selective side group dissociation.

6. Acknowledgments

This work is supported by Swedish Research Council (Contract No. 2015-06501). Facility is supported by the Swedish National Infrastructure for Computing (SNIC). We acknowledge the European Union (EU) and Horizon 2020 funding awarded under the Marie Skłodowska Curie action to the EUROPAH consortium, grant number 722346. Studies of interstellar PAHs at Leiden Observatory are supported through a Spinoza award.

References

G. G. M. Tielens, *Annu. Rev. Astron. Astrophys.*, 2008, **46**, 289.

A. G. G. M. Tielens, The Physics and Chemistry of the Interstellar Medium, *Cambridge Univ Press, Cambridge, UK*, 2005.

M. P. Bernstein, J. E. Elsila, J. P. Dworkin, S. A. Sandford, L. J. Allamandola & R. N. Zare, *Astrophys. J.*, 2002, **576**, 1115.

A. I. S. Holm, H. A. B. Johansson, H. Cederquist, & H. Zettergren, *J. Chem. Phys.*, 2011, **134**, 044301.

T. Chen, M. Gatchell, M. H. Stockett, R. Delaunay, A. Domaracka, E. R. Micelotta, A. G. G. M. Tielens, P. Rousseau, L. Adoui, B. A. Huber, H. T. Schmidt, H. Cederquist, & H. Zettergren, *J. Chem. Phys.*, 2015, **142**, 144305.

O. Berné, & A. G. G. M. Tielens, *Proc. Natl. Acad. Sci., & USA*, 2012, **109**, 401.

J. Zhen, P. Castellanos, D. M. Paardekooper, H. Linnartz, & A. G. G. M. Tielens, *Astrophys. J. Lett.*, 2014, **797**, L30.

R. Walsh, *Chem. Soc. Rev.*, 2008, **37**, 686.

H. W. Jochims, H. Baumgartel, & S. Leach, *Astrophys. J.*, 1999, **512**, 500.

M. Rapacioli, A. Simon, C. C. M. Marshall, J. Cuny, D. Kokkin, F. Spiegelman, & C. Joblin, *J. Phys. Chem. A*, 2015, **119**, 12845.

J. Zhen, P. Castellanos, H. Linnartz, & A. G. G. M. Tielens, *Mol. Astrophys.*, 2016, **5**, 1.

C. Lifshitz, *Int. Rev. Phys. Chem.*, 1997, **16**, 113.

J. Zhen, D. M. Paardekooper, A. Candian, H. Linnartz, & A. G. G. M. Tielens, *Chem. Phys. Lett.*, 2014, **592**, 211.

M. V. Doroshenko, & R. J. Cotter, *Rapid Commun. Mass Spectrum.*, 1996, **10**, 65.

A. P. Scott, & L. Radom, *J. Phys. Chem.*, 1996, **100**, 16502.

J. H. Beynon, G. R. Lester, & A. E. Williams, *J. Phys. Chem.*, 1959, **63**, pp 1861

A. J. de Haas, J. Oomens, & J. Bouwmana, *Phys. Chem. Chem. Phys.*, 2017, in press, **DOI: 10.1039/C6CP08349H**.